AIMS Materials Science, 6(1): 80–96.
DOI: 10.3934/matersci.2019.1.80
Received: 13 October 2018
Accepted: 13 January 2019
Published: 02 February 2019

http://www.aimspress.com/journal/Materials

Research article

Optimization on dry sliding wear behavior of yellow brass using face centered composite design

Subbarayan Sivasankaran*

Department of Mechanical Engineering, Qassim University, Buraydah, Saudi Arabia

* **Correspondence:** Email: sivasankarangs1979@gmail.com, sivasankaran@qec.edu.sa, s.udayar@qu.edu.sa; Tel: +9660534810975.

Abstract: The proposed research has investigated the dry sliding wear behavior at ambient temperature atmosphere on yellow brass intended for locks, gears, bearings, ammunition casings, and valves. The experiments were conducted based on the central composite design. The wear experiments were performed using the pin-on-disc tribometer by varying the applied load, the sliding velocity, and the sliding distance. The obtained wear results were examined using the multiple regression non-linear model and then the results were validated by performing the confirmation test. It was found that the predicted wear based on the developed regression model was well correlated with the confirmation results. Further, the detailed microstructures of as-received and worn surfaces were examined and reported. In addition, the plotted surface graphs between the input independent parameters and the responses showed that the wear rate started to vary linearly with the function of load whereas it was varied non-linearly with the function of the sliding velocity and the sliding distance.

Keywords: copper alloys; sliding wear; optimization; response surface methodology; worn morphology

1. Introduction

In recent years, the non-ferrous alloys have played a major role in the manufacturing of most of the commodity items in which the brass (one of the copper-based alloys) is being applied more. The brass is consisting of copper (Cu) and zinc (Zn) elements [1–5]. The amount of incorporation of Zn element with the Cu has formed several types of brasses with different properties. The major

applications of brasses are in the radiator tubes, the hydraulic brake tubes, the journal bearings, the carburetor, the fasteners, and in marine components [3,6–9]. The properties of brass can be enhanced by cold working which is available in different mechanical properties. Almost all the brasses have been excellent in corrosion resistance, higher in malleability, and have a relatively low melting point. Among the several brasses, the yellow brass has provided superior strength, more ductility and good casting properties which are necessary for the manufacturing of ornaments. Yellow brass is the alloy of 65% Cu and 35% Zn [10]. In real applications, the components made up of brasses have been subjected to mechanical rubbing action which creates abrasive action. Wear is one kind of metal removal from the contacting surfaces due to relative motions between the two mating parts [11,12]. The wear that occurred in the components was mainly based on the applied load, the operating temperature, the speed, the hardness of the alloy, the time duration of mechanical action, the atmospheric action, and the presence of foreign matters. Wear is a foremost issue in the engineering field in which 1 to 4% of gross national product (GNP) has consumed more direct cost during the usage of mechanical parts. Therefore, it is necessary to examine and study the wear behavior of brasses and its alloys [13–15].

Tribological behavior, namely the wear rate, the wear resistance, and the coefficient of friction, has clarified the wear rate of materials which have played a major role in material removal [5–9,16]. This indicates the transfer of material from one surface to another owing to the relative motion between the contacting surfaces. A dry sliding wear test is the best experimental technique for many structural applications to find out the wear behavior. However, to explore in detail the wear behavior of any material, it is necessary to conduct a number of experiments in the conventional one-to-one method. This conventional method has needed more investment, but these issues can be solved by implementing the design and analysis of experimental technique by which the number of experiments can be minimized by considering more input parameters. The response surface methodology (RSM) is a powerful statistical tool employed to understand the performance of the process when multiple parameters are involved [8–14]. This technique has reduced the experimental time with the minimum number of experiments and it has a series of steps such as the prediction of the response for different combinations of parameters, development of regression coefficients estimation, fitting of the experimental data, prediction of response and checking the adequacy of the fitted model. The analysis can be carried out for a 95% confidence level and 5% significance level to determine the significance of the input parameters employed for the construction of the model [15]. The significance of the regression model, linear, square and interaction terms, as well as the lack of fit, can be known through this analysis. In order to ensure the consistency among the results, the central composite design (CCD) has paved a way by providing 6 numbers of experimental runs with the same process parameter which cannot be done through Box-Behnken, Taguchi and genetic algorithm methods [17–24]. Based on the literature, there was no report and detailed study on the dry sliding wear behavior of yellow brasses. Therefore, the present research work was focused to optimize the essential wear parameters such as the load, the sliding velocity and the sliding distance using central composite design in RSM technique to determine the appropriate input parameters to be used for the brass components/parts in real time applications which minimize the wear.

2. Experimental methodology and optimization technique

2.1. Yellow brass sample preparation and characterization

The hot rolled commercial yellow brass was purchased from Kovai Metal Mart (P) Ltd., India. The chemical composition, the physical properties and the mechanical properties of as-received yellow brass are given in Table 1. The as-received yellow brass is a face-centered cubic (FCC) crystal system which usually consists of α-phase (majority) and some amount of β-phase. The microstructural images in as-received condition and the worn surfaces were examined using the FESEM (field emission scanning electron microscope) of S-3400 N, Hitachi, with the EDS (energy dispersive spectrometer) of XFlasj 5010, Bruker. The as-received hot rolled yellow brass was cut into several pieces of ø10 × 30 mm as pins for doing the wear test. Before, the samples were cleaned with acetone and then the samples were polished as per the metallographic procedure. The samples were mounted in a Bakelite thermosetting agent, polished with different SiC grit papers (400, 600, 800, 1000, 1200, 2000 SiC grits/inch^2), and finally, the samples were lapped by 3 μm alumina paste. After polishing, the super finish samples were etched using HNO_3 (50 mL) and distilled water (50 mL) to examine the microstructure.

Table 1. Physical and mechanical properties of as-received yellow brass.

Parameter(s)		Description(s)
Chemical composition		Cu = 65%, Zn = 35%
Physical properties	Density, ρ	8.42 g/cm^3
	Melting point	900 ℃
	Coefficient of thermal expansion	20.1 μm/m ℃
	Thermal conductivity	112 W/mK
Mechanical properties	Hardness (HR30T)	16.5
	Ultimate tensile strength	320 MPa
	Tensile yield strength	105 MPa
	Elongation at failure	62%
	Rockwell hardness	55 HRF

2.2. Dry sliding wear test

The pin-on-disc sliding wear test equipment was used to study the tribological behavior of yellow brass under the dry condition at ambient temperature. Figure 1a shows the photograph of the pin-on-disc (supplied by DUCOM, India) wear test apparatus which consists of the counter disc, the sample holder, the sample, the applied load, the data acquisition system, and the data monitoring system. Further, the schematic of the sliding wear test is also shown in Figure 1b. The cylindrical counter disc was made of hardened stainless steel having 5 mm thickness and 100 mm diameter. The counter disc was initially ground and cleaned with acetone to eliminate the presence of oxide layers, foreign particles, and moisture. The prepared samples for wear test were weighed before and after

the test by which the mass loss was determined. Based on the mass losses, the wear rate and the volume loss were determined using the following formula:

$$\text{Wear rate}\left(\frac{\text{mm}^3}{\text{m}}\right) = \frac{\text{Volume loss (mm}^3\text{)}}{\text{sliding distance (m)}} \times 1000 \quad (1)$$

$$\text{Volume loss (mm}^3\text{)} = \frac{\text{Weight loss (g)}}{\text{Density}\frac{\text{(g)}}{\text{(cm}^3\text{)}}} \quad (2)$$

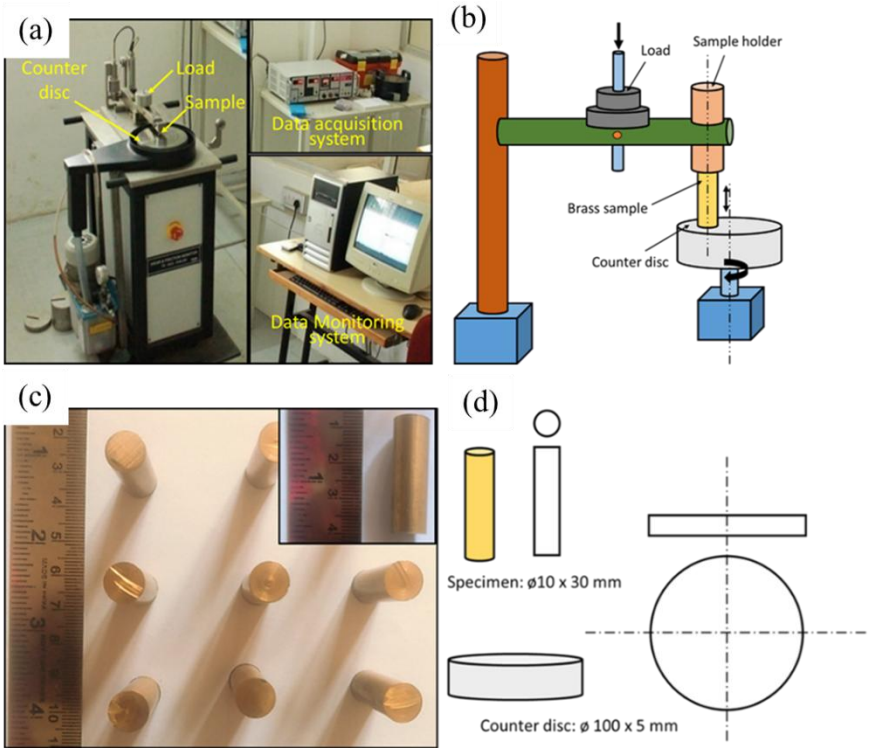

Figure 1. (a) Photograph of sliding wear test apparatus; (b) the schematic of sliding wear test; (c) photograph of yellow brass samples before sliding wear; (d) the dimensions of the counter disc and the pin.

2.3. Design of experiments

The wear test was conducted by varying the loads (10 N, 30 N and 50 N), the sliding velocities (1 m/s, 3 m/s and 5 m/s), and the sliding distances (500 m, 1500 m, and 2500 m). The experiments were conducted as per the face-centered central composite design (FCCD). The three independent input parameters with three levels were illustrated in Table 2. The photograph of yellow brass samples of before wear is shown in Figure 1c. Minitab (v15) statistical software was used to perform the design of experiments and analyses. In the FCCD, twenty experimental runs were used with three input parameters at three levels. The actual experimental design and the corresponding response are illustrated in Table 3. At least three replicas were used in each input condition and the average was used for the investigation. The analysis of variance (ANOVA) was applied to investigate the significant parameters and the individual parameter's percentage contribution. The input independent parameters (the load, the sliding velocity and the sliding distance) and the corresponding responses

(the wear rate, and the coefficient of friction) were correlated by means of second ordered mathematical regression models which are expressed as below:

$$Y_u = b + \sum b_i X_{iu} + \sum b_{ii} X_{iu}^2 + \sum b_{ij} X_{iu} X_{ju} \quad (3)$$

where, Y_u is the response, b, b_i, b_{ii} and b_{ij} are the regression model coefficients. The above polynomial equation has indicated the linear effect (second term), square effect (third term), and the interaction effect (third term). The influence of input parameters on the responses was studied through the contour plots which were expected to minimize the wear rate and the coefficient of friction. In the present study, the experimental parameters were chosen based on commercial experiences. Based on the results, the optimum input parameter could be selected by which the wear of the yellow brass components could be diminished in the real dynamic applications.

Table 2. Wear parameters and their levels used in pin-on-disc tribometer.

Parameter	Units	Notation	Level		
Load	(N)	L	10	30	50
Velocity	(m/s)	V	1	3	5
Sliding distance	(m)	SD	500	1500	2500

Table 3. Design matrix and experimental results on sliding wear of yellow brass.

Experiment number	Load, N	Velocity, m/s	Distance, m	Wear rate, mm^3/m	Coefficient of friction, μ
1	30	3	2500	0.002044	0.882
2	10	5	2500	0.000457	0.917
3	30	3	500	0.004040	0.829
4	30	1	1500	0.003701	0.702
5	30	3	1500	0.002387	0.682
6	30	3	1500	0.002327	0.678
7	50	5	500	0.001730	0.952
8	30	3	1500	0.002332	0.681
9	50	1	2500	0.003516	0.866
10	10	1	500	0.003954	0.902
11	30	3	1500	0.002339	0.679
12	50	1	500	0.006020	0.867
13	10	5	500	0.000762	0.939
14	10	3	1500	0.001461	0.735
15	30	3	1500	0.002347	0.68
16	10	1	2500	0.002380	0.853
17	50	5	2500	0.001192	0.97
18	30	5	1500	0.000727	0.851
19	30	3	1500	0.002341	0.679
20	50	3	1500	0.002914	0.788

3. Results and discussion

3.1. Microstructural examination

Before the wear test, the SEM microstructure of as-received and the hot rolled brass are shown in Figure 2. From Figure 2a, more quantity of α-phases were observed and some amount of β-phases which were all related to the yellow brass. The white region indicated the α-phases (primary phase) and the dark grey region indicated the β-phases (secondary phase). The observed grains were almost equiaxed with random oriented ones which further showed the homogeneous nature. Based on several microstructural images, the average grain sizes were calculated for both the α-phase and β-phase. The average grain size of α-Cu phase was around 40 ± 5.3 μm which was calculated from 500 grains. In a similar manner, the average grain size of β-Zn phase was also computed from 200 grains which were around 22 ± 2.6 μm. In fact, the solid crystals with random orientation would have isotropic properties [4]. The energy dispersive spectroscopy (EDS) of the SEM (Figure 2b) also confirmed the presence of copper and zinc phases, and the chemical composition in terms of weight percentage [3,4] has well correlated with Table 1.

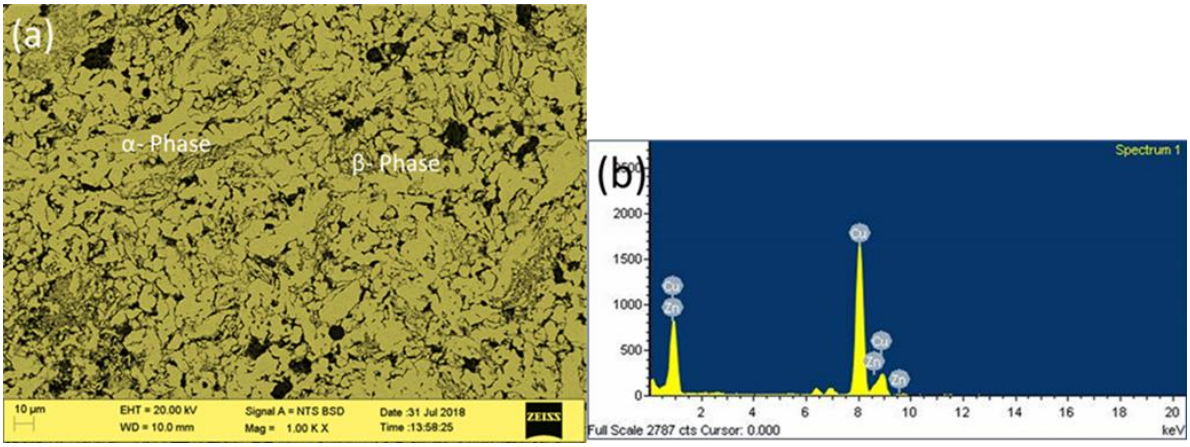

Figure 2. (a) SEM microstructure of as-received yellow brass; (b) corresponding EDS.

The electron backscattered diffraction (EBSD) analyses were also carried out for the as-received yellow brass using FEI Quanta FEG SEM with TSL-OIM software to the colored grain distribution of α-Cu phase and β-Zn phase (Figure 3a). The corresponding inverse pole figure is also shown as inset of Figure 3a at the bottom left corner. Further, Figure 3b shows the pole figure in terms of mean uniform density (MUD) which indicated that one preferred texture orientation was observed in the legend of (1 1 0) that corresponds to {2 2 0} planes. In addition, from Figure 3c, binomial grain misorientation angle distribution (low angle grain boundaries and high-angle grain boundaries) was also observed which was expected in the presence of α-Cu phase and β-Zn phase.

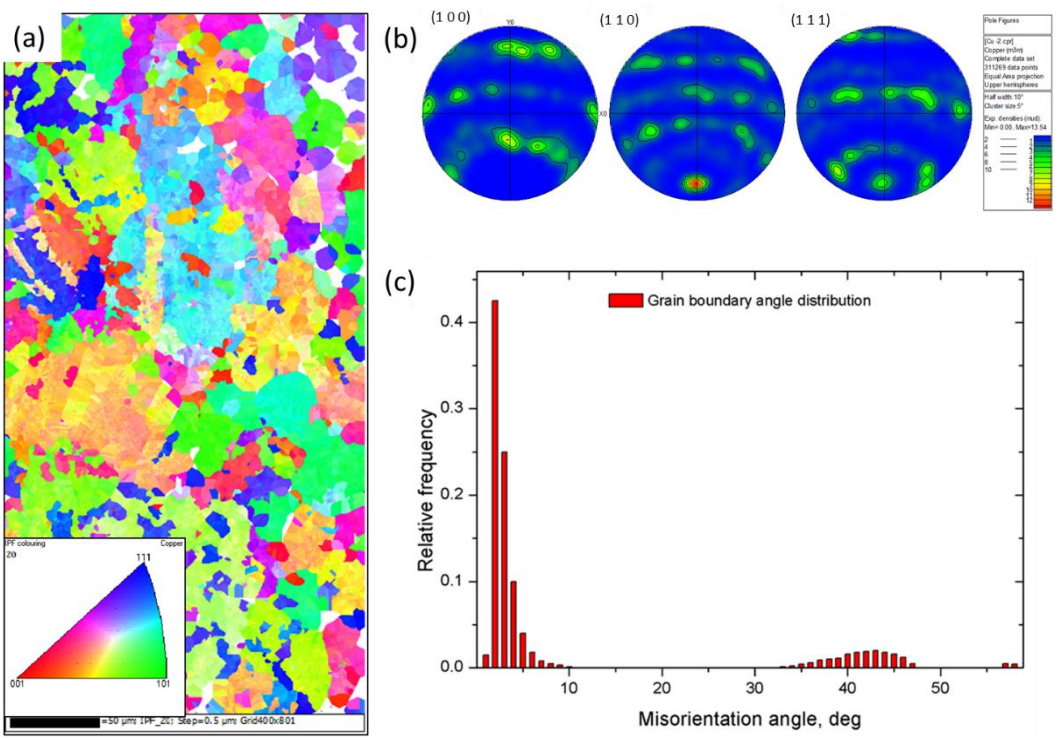

Figure 3. (a) EBSD grain coloured maps of as-received yellow brass, inset at the bottom shows the inverse pole figure; (b) the pole figure of (a) indicates the texture orientation; (c) grain misorientation angle distribution.

3.2. Investigation on dry sliding wear behavior on yellow brass

3.2.1. Influence of input variables on the wear rate

Table 3 illustrated the wear rate and the coefficient of friction of yellow brass with the function of process parameters. The results revealed that the experiment number 2 exhibited the minimum wear rate of 0.000457 mm^3/m with the applied load of 10 N, the sliding velocity of 5 m/s, and the sliding distance of 2500 m. The minimum coefficient of friction of 0.687 was obtained in experiment number 6 with the applied load of 30 N, the sliding velocity of 3 m/s, and the sliding distance of 1500 m. Based on these values, the optimum input parameters could be predicted which are near to the optimum region. However, these parameters would not be the optimum. The developed mathematical non-linear regression model (polynomial) is given in Eq 4 which can be used to predict the wear rate for the given input process parameters.

$$\begin{aligned} Wear\ rate\ (mm^3/m) = {} & 0.00051317 + (0.0000942) \times Load - \\ & (0.0005637) \times Velocity - (0.0000029) \times Distance - \\ & (0.000000624) \times Load \times Load - (0.0000557) \times Velocity \times Velocity + \\ & (0.000000000605) \times Distance \times Distance - (0.00000468) \times Load \times Velocity - \\ & (0.00000000728) \times Load \times Distance + (0.000000202) \times Velocity \times Distance \\ & R^2 = 98.947\%,\ R^2(adj) = 98.04\% \end{aligned} \quad (4)$$

The various main factors (the load, the sliding velocity, and the sliding distance) and the corresponding interaction effect were taken for the investigation which was further classified into two categories such as significant factors and non-significant factors. The decision of whether the factor is significant and or non-significant was made based on the P-value of 0.05 which has a confidence level of 95%. If the p-value is less than 0.05, then the corresponding factor would give a major effect on the response which is called significant factor, and otherwise, the particular input parameter is called an insignificant factor. Table 4 illustrated the observed ANOVA results on the wear rate during the sliding wear test on yellow brass which indicated that almost all the linear terms, square terms, and the interaction terms were influenced much on the wear rate. Further, the developed regression model (Eq 4) was the R^2 value of 98.947% and the adjusted R^2 value of 98.04% which meant the developed model has more accuracy. From Table 4 and the model (Eq 4), among the linear terms, the sliding velocity was influenced much followed by the distance and the load. In a similar manner, among the square terms, only the square of distance was influenced much, little effect was produced by the square of the load, and the square of velocity was not influenced. Further, among the interaction terms, the term "Velocity × Distance" was influenced much followed by the terms of "Load × Velocity" and "Load × Distance".

Table 4. ANOVA test results for wear rate during sliding wear test on yellow brass.

Source	DF	Seq SS	Adj SS	Adj MS	F	P
Regression	9	0.000033	0.000033	0.000004	106.49	<0.0001
Linear terms	3	0.00003	0.00003	0.00001	292.85	<0.0001
Load (N)	1	0.000004	0.000004	0.000004	116.64	<0.0001
Velocity (m/s)	1	0.000022	0.000022	0.000022	623.84	<0.0001
Distance (m)	1	0.000005	0.000005	0.000005	138.08	<0.0001
Square terms	3	0.000001	0.000001	0.000000	9.71	0.0030
Load × Load	1	0.000000	0.000000	0.000000	4.94	0.0510
Velocity × Velocity	1	0.000000	0.000000	0.000000	3.94	0.0750
Distance × Distance	1	0.000001	0.000001	0.000001	29.07	0.0000
Interaction	3	0.000002	0.000002	0.000001	16.92	<0.0001
Load × Velocity	1	0.000000	0.000000	0.000000	8.1	0.0170
Load × Distance	1	0.000000	0.000000	0.000000	4.89	0.0510
Velocity × Distance	1	0.000001	0.000001	0.000001	37.76	<0.0001
Residual Error	10	0.000000	0.000000	0.000000		
Lack-of-Fit	5	0.000000	0.000000	0.000000	151.34	<0.0001
Pure Error	5	0.000000	0.000000	0.000000		
Total	19	0.000034				

Figure 4 explained the contour plots of wear rate during the sliding wear test on yellow brass at room temperature. From Figure 4a, the results indicated that the wear rate started to increase gradually when the function of the applied load for any sliding velocity remained constant. These results were attributed to the formation of more thrust forces between the pin (yellow brass) and the counter disc, and consequently, the materials were expected to decrease. However, at the lower load,

when the velocity started to increase, the amount of formed thrust force was expected to be less and hence, less wear loss in the materials was expected to occur. In contrast, for instance, at higher load and higher value of sliding velocity, less wear rate was observed which was attributed to the domination of slipping phenomenon [25,26]. In general, as the sliding velocity was increased, the introduced/increased rotational forces in the materials were forced to move the sample in a faster manner, which might be expected to form the slippage called slipping phenomenon that nullified the thrust forces. Hence, less wear rate occurred at high velocity with a high load. The contour plot of Figure 4b drawn between the load and the sliding distance showed the similar behavior of Figure 4a. At a lower value of sliding distance, the wear rate started to increase gradually with the function of load due to the domination of thrust forces.

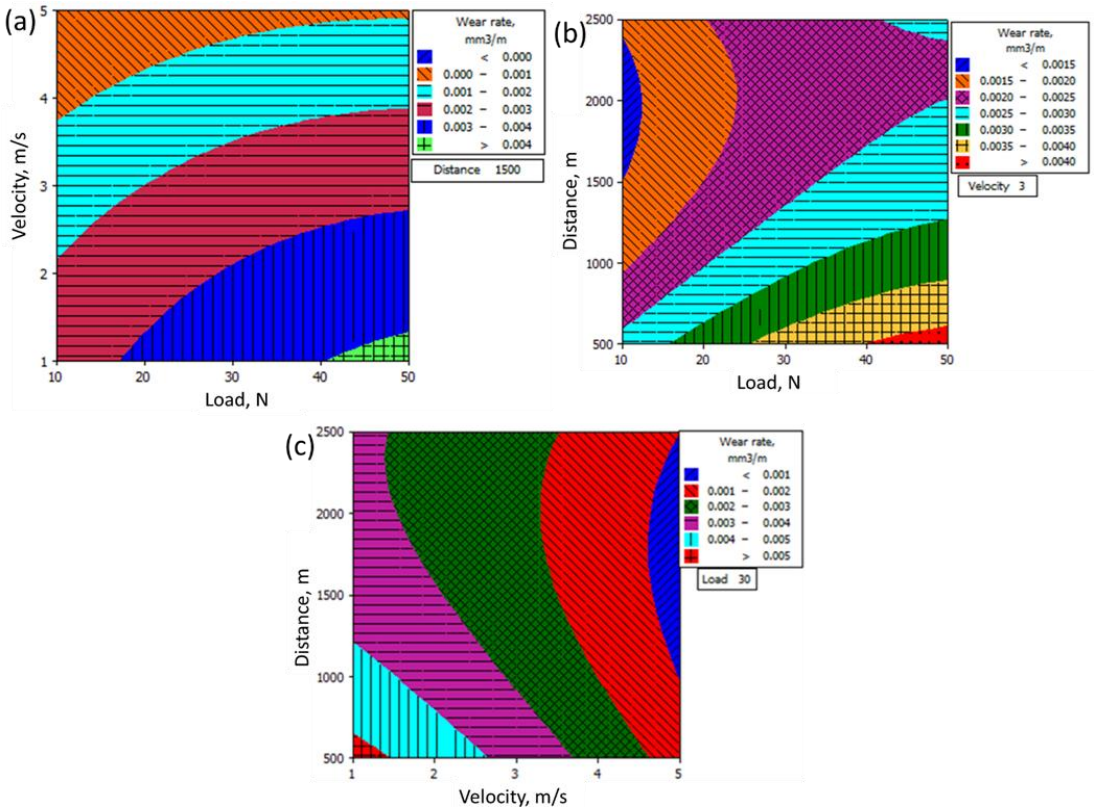

Figure 4. Contour plots of the wear rate of commercial yellow brass with the function of: (a) velocity vs. load; (b) distance vs. load; (c) distance vs. velocity.

However, at a higher value of sliding distance and at higher load, the observed wear rate increased due to more contact time of the sample over the counter disc and hence, more volume loss occurred. The result of Figure 4c revealed that the observed wear was more at a low velocity which was attributed to more adhesion and more contact time taken by the sample over the counter disc. Due to this, more plastic deformation occurred in the sample which led to more wear loss. However, at high velocity, the contact time between the sample and the counter disc decreased and hence, less wear occurred. According to Archard's law, the applied load and the sliding distance are directly proportional and influence the wear rate. Therefore, in the present work, the wear rate was highly influenced by the function of the load and the distance.

3.2.2. Influence of input variables on the coefficient of friction

The coefficient of friction could be predicted by the following mathematical non-linear regression model which is given in Eq 5.

$$\begin{aligned}&\text{Coefficient of friction (CoF)} = 1.16854 - (0.00657) \times \text{Load} - \\&(0.06711) \times \text{Velocity} - (0.000415) \times \text{Distance} + \\&(0.00009) \times \text{Load} \times \text{Load} + (0.01275) \times \text{Velocity} \times \text{Velocity} + \\&(0.00000013) \times \text{Distance} \times \text{Distance} + (0.000275) \times \text{Load} \times \text{Velocity} + \\&(0.00000055) \times \text{Load} \times \text{Distance} + (0.00000288) \times \text{Velocity} \times \text{Distance} \\&R^2 = 94.64\%,\ R^2\ (\text{adj}) = 89.74\%\end{aligned} \quad (5)$$

Table 5 showed the observed ANOVA results on the coefficient of friction during the sliding wear test on yellow brass which indicated that the sliding velocity in the linear term was only highly influenced when compared to the other two linear terms. In the square terms, the square of distance was influenced much followed by the square of velocity. However, the square term of the load was not influenced in the coefficient of friction. Further, no interaction term has not influenced the coefficient of friction. Further, the developed regression model (Eq 5) possessed the R^2 value of 94.64% and the adjusted R^2 value of 89.74% which meant the developed model had more accuracy.

Table 5. ANOVA test results for the coefficient of friction during sliding wear test on yellow brass.

Source	DF	Seq SS	Adj SS	Adj MS	F	P
Regression	9	0.205275	0.205275	0.022808	19.47	<0.0001
Linear terms	3	0.020213	0.020213	0.006738	5.75	0.0150
Load (N)	1	0.000941	0.000941	0.000941	0.8	0.3910
Velocity (m/s)	1	0.019272	0.019272	0.019272	16.45	0.0020
Distance (m)	1	0.000000	0.000000	0.000000	0.000	0.9930
Square terms	3	0.182861	0.182861	0.060954	52.03	<0.0001
Load × Load	1	0.104546	0.003564	0.003564	3.04	0.112
Velocity × Velocity	1	0.03184	0.007153	0.007153	6.11	0.033
Distance × Distance	1	0.046475	0.046475	0.046475	39.67	<0.0001
Interaction	3	0.002201	0.002201	0.000734	0.63	0.614
Load × Velocity	1	0.000968	0.000968	0.000968	0.83	0.385
Load × Distance	1	0.000968	0.000968	0.000968	0.83	0.385
Velocity × Distance	1	0.000265	0.000265	0.000265	0.23	0.645
Residual Error	10	0.011716	0.011716	0.001172		
Lack-of-Fit	5	0.011705	0.011705	0.002341	1080.5	<0.0001
Pure Error	5	0.000011	0.000011	0.000002		
Total	19	0.000034				

Figure 5 showed the contour plot of the coefficient of friction with the function of the applied load, the sliding velocity, and the sliding distance. The result of Figure 5a explained that the average

range of coefficient of friction value (0.700 to 0.725) was observed at the lower value of the applied load and the lower value of sliding velocity. At the middle value of the load, the observed coefficient of friction was low (<0.7). This meant the value of the coefficient of friction started to decrease with the function of the load up to the middle one which was attributed to less frictional force occurring. However, when the applied load and the sliding velocity increased further, the coefficient of friction increased due to a higher amount of thrust force which was caused by the increase of the load, and hence, a more frictional force due to heavy contact of the sample over the counter disc occurred. The result of Figure 5b demonstrated that the observed coefficient of friction value increased with the function of the load and the sliding distance. These results were attributed to more material contact with the disc and more time. This more material contact was expected to produce more plastic deformation which led to increasing the frictional forces. Similar behavior was observed in the result of Figure 5c.

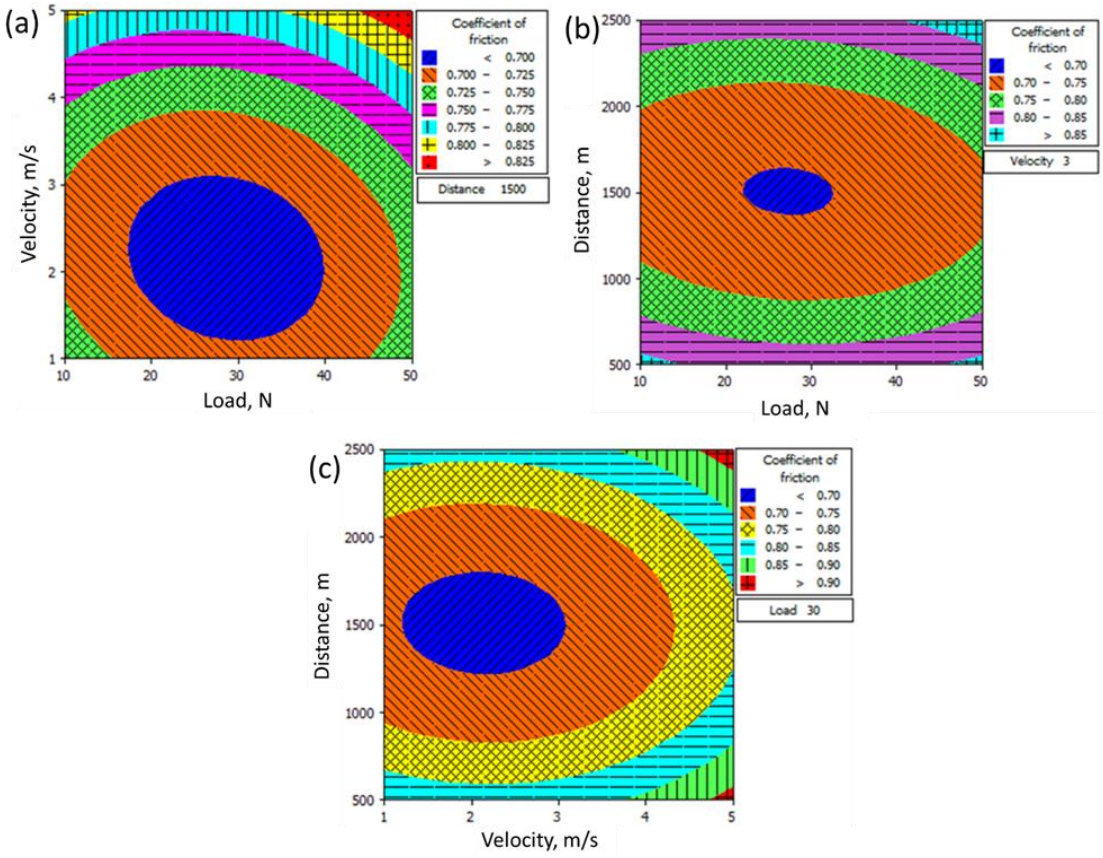

Figure 5. Contour plots of the coefficient of commercial yellow brass with the function of (a) velocity vs. load; (b) distance vs. load; (c) distance vs. velocity.

Figure 6 depicted the normal probability plot of dry sliding wear behavior of yellow brass. The plot demonstrated that the maximum number of the residuals has coincided over the inclined fitted line which explained clearly the strong correlation between the model's prediction and the experimental one.

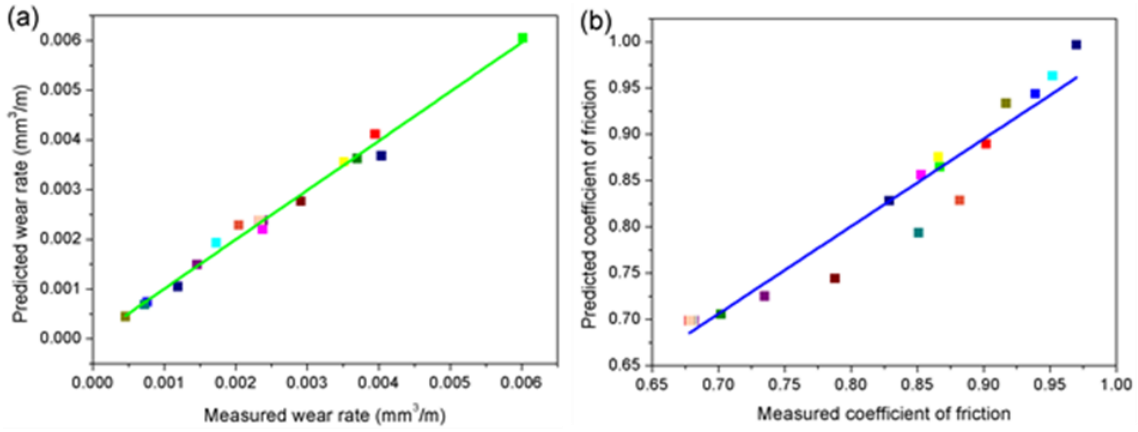

Figure 6. The measured and the predicted values on dry sliding wear behavior of yellow brass: (a) wear rate; (b) the coefficient of friction.

3.2.3. Confirmatory test

Table 6 illustrated the measured, the predicted results of the wear rate, and the coefficient of friction which was computed based on the confirmatory test and the developed mathematical polynomial model. From Table 6, it was clearly shown that all the predicted values were much closer to the experimental ones with a 95% confidence level.

Table 6. Confirmation experiment and regression wear rate.

Load (N)	Velocity (m/s)	Sliding distance (m)	Wear rate (mm^3/m)			Coefficient of friction		
			Experimental Wear rate (mm^3/m)	Regression Wear rate (mm^3/m)	Error (%)	Experimental Wear rate (mm^3/m)	Regression Wear rate (mm^3/m)	Error (%)
15	2	750	0.003153	0.003300	4.655	0.7734	0.78765	1.85
15	2	900	0.002893	0.003059	5.74	0.7401	0.7596	2.65
10	4	750	0.001490	0.001394	6.40	0.8012	0.8330	3.97

3.2.4. Optimization of the responses

The main feature of implementing the response surface methodology is that the optimization of all the responses based on the input parameters can be carried out. It is well known that the wear rate and the coefficient of friction mainly influenced the applied sliding parameters in the real-time applications based on which the service life of the components could be designed. It is necessary to do the optimization when we want to increase the service life the components. In the present research work, the wear rate and the coefficient of friction were optimized using the response optimization tool in the Minitab software. Both of these two responses were minimized, and hence, the target values were fixed based on minimum criteria function. Figure 7 showed the optimized plot of the two responses. From Figure 7, the optimum input parameters were the applied load of 28.5859 N, the

sliding velocity of 2.1717 m/s, and the sliding distance of 1510.1010 m with the desirability of 0.99262.

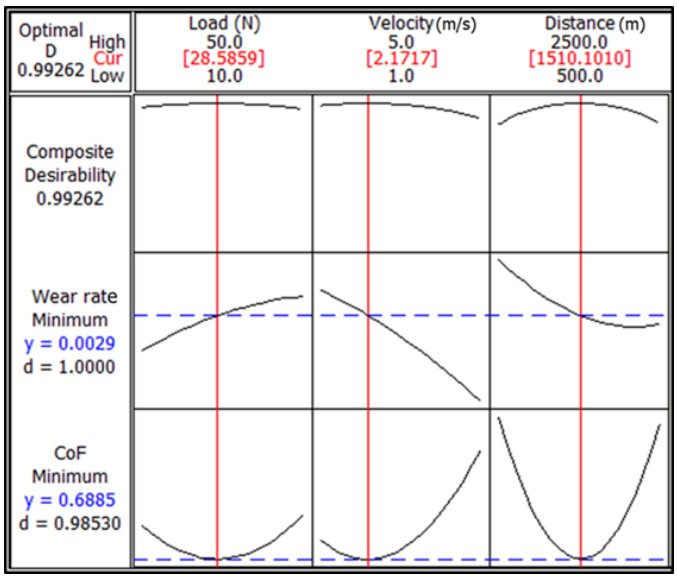

Figure 7. Optimal conditions of process parameters during sliding wear test on yellow brass.

3.3. Worn surface morphology

Figure 8 showed the worn surface morphology of the sample with the function of load. It was clearly known that a lesser amount of cutting effect, the abrasion effect, and the plowing effect were observed when the load was 10 N. However, when the load started to increase, more amount of cutting lines, abrasion effect, and the plowing effect was formed due to more contact of the sample with the counter disc which was expected to introduce more friction [27,28]. Therefore, more plastic deformation has occurred at higher load which produced more damages in the sample. Figure 9 showed the worn surface morphology of the sample with the function of the sliding velocity and the distance. At a lower load and lower value of sliding velocity, severe debris, scratches, and plowing were observed in the sample due to more sample contact time with the counter disc. However, as the velocity increased, a good surface morphology was obtained. This result was attributed to the fact that the sample contact time started to decrease as the velocity increased which led to producing less wear [25,26]. These results were clearly seen in Figure 9b,c. Figure 10 showed the worn surface morphology of the optimized sample which was a good surface with little damages like the scratches, plowing, pitting, debris, etc. The energy spectroscopy of the optimized sample was also shown in Figure 10b which confirmed the presence of alloy system and some iron oxide particles which were expected to form from the chemical composition of the counter disc.

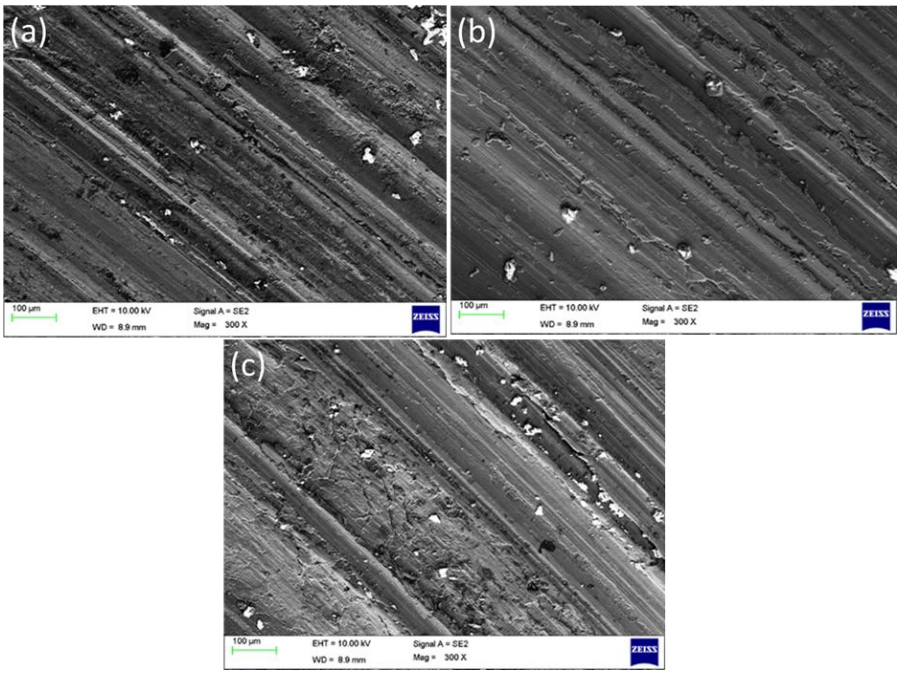

Figure 8. The worn surface morphology of dry sliding wear behavior of yellow brass with the function of the applied load: (a) load = 10 N, velocity = 1 m/s, distance = 500 m, Exp.No.10; (b) load = 30 N, velocity = 1 m/s, distance = 1500 m, Exp.No.4; (c) load = 50 N, velocity = 1 m/s, distance = 500 m, Exp.No.12.

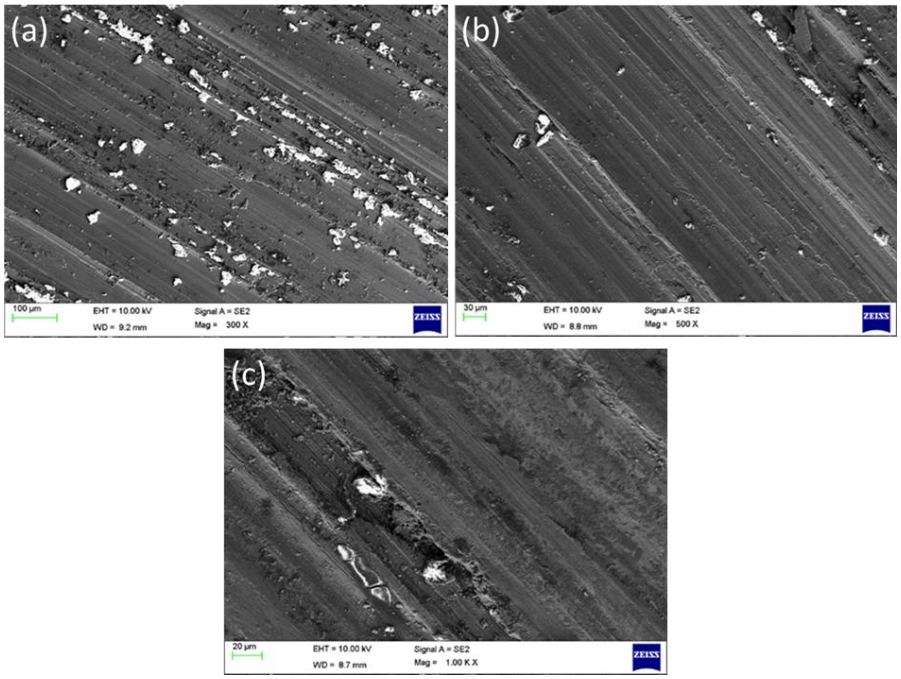

Figure 9. The worn surface morphology of dry sliding wear behavior of yellow brass with the function of the sliding velocity: (a) load = 10 N, velocity = 1 m/s, distance = 2500 m, Exp.No.16; (b) load = 10 N, velocity = 3 m/s, distance = 1500 m, Exp.No.14; (c) load = 10 N, velocity = 5 m/s, distance = 500 m, Exp.No.13.

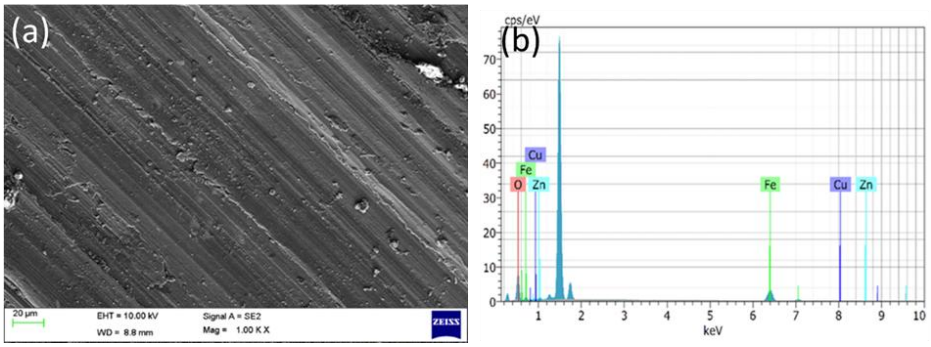

Figure 10. Worn surface morphology at the optimum condition with corresponding EDS analysis.

4. Conclusions

The sliding wear test on the commercial yellow brass was successfully conducted and the optimum process parameters were determined. From the present study, the following conclusions were drawn.

- The empirical relationship between the process parameters and the responses using the face-centered composite design was developed which can be used to examine the factor of the load, the sliding velocity and sliding distance on the wear rate and the coefficient of friction.
- The present research work can be used to predict the wear rate and the coefficient of friction at 5% significant level.
- The optimum value of wear rate was achieved at the applied load of 28.5859 N, the sliding velocity of 2.1717 m/s, and the sliding distance of 1510.1010 m with the desirability of 0.99262.
- Investigations with FESEM and EDAX had ensured the presence of some iron oxide particles in the base metal which might be expected to form from the counter disc.
- ANOVA results exposed that the sliding distance has a greater impact on the wear rate.

Acknowledgments

The corresponding author wishes to thank the Qassim University for all funding and support required to carry out this research.

Conflicts of interest

The author declares no conflict of interest.

References

1. Bénard AEB, Hernández DM, Reyes JGG, et al. (2014) Synthesis, characterization and cold workability of cast copper-magnesium-tin alloys. *Metall Mater Trans A* 45: 555–562.
2. Taha MA, El-Mahallawy NA, Hammouda RM, et al. (2012) Machinability characteristics of lead free-silicon brass alloys as correlated with microstructure and mechanical properties. *Ain Shams Eng J* 3: 383–392.

3. Kong XL, Qiao LJ, Liu YB (2003) Wear behavior of nanocrystalline Cu-Zn alloy. *J Mater Eng Perform* 12: 312–316.
4. Sivasankaran S, Alaboodi AS, Al-Mufadi F (2018) Cold deformation of dezincification resistant yellow brass for plumbing applications. *Mater Manuf Process* 33: 1693–1700.
5. Neishi K, Horita Z, Langdon TG (2001) Achieving superplasticity in a Cu–40% Zn alloy through severe plastic deformation. *Scripta Mater* 45: 965–970.
6. Zhang ZJ, An XH, Zhang P, et al. (2013) Effects of dislocation slip mode on high-cycle fatigue behaviors of ultrafine-grained Cu–Zn alloy processed by equal-channel angular pressing. *Scripta Mater* 68: 389–392.
7. Vinogradov A, Vasilev E, Seleznev M, et al. (2016) On the limits of acoustic emission detectability for twinning. *Mater Lett* 183: 417–419.
8. Tarasov SY, Filippov AV, Kolubaev EA, et al. (2017) Adhesion transfer in sliding a steel ball against an aluminum alloy. *Tribol Int* 115: 191–198.
9. Filippov AV, Nikonov AY, Rubtsov VE, et al. (2017) Vibration and acoustic emission monitoring the stability of peakless tool turning: Experiment and modeling. *J Mater Process Tech* 246: 224–234.
10. Kato H, Todaka Y, Umemoto M, et al. (2015) Sliding wear behavior of sub-microcrystalline pure iron produced by high-pressure torsion straining. *Wear* 336–337: 58–68.
11. Konkova T, Mironov S, Korznikov A, et al. (2015) An EBSD investigation of cryogenically-rolled Cu–30% Zn brass. *Mater Charact* 101: 173–179.
12. Kalita K, Shivakoti I, Ghadai RK (2017) Optimizing process parameters for laser beam micro-marking using genetic algorithm and particle swarm optimization. *Mater Manuf Process* 32: 1101–1108.
13. Shah KB, Kumar S, Dwivedi DK (2007) Aging temperature and abrasive wear behaviour of cast Al–(4%, 12%, 20%) Si–0.3% Mg alloys. *Mater Design* 28: 1968–1974.
14. Tang C, Wang JM, Wen GW, et al. (2011) Bauschinger effect in wear of Cu–40Zn alloy and its variations with the wear condition. *Wear* 271: 1237–1243.
15. Mousavi SE, Meratian M, Rezaeian A (2017) Investigation of mechanical properties and fracture surfaces of dual-phase 60–40 brass alloy processed by warm equal-channel angular pressing. *J Mater Sci* 52: 8041–8051.
16. Kim HS, Kim WY, Song KH (2012) Effect of post-heat-treatment in ECAP processed Cu–40% Zn brass. *J Alloy Compd* 536: S200–S203.
17. Seeman M, Ganesan G, Karthikeyan R, et al. (2010) Study on tool wear and surface roughness in machining of particulate aluminum metal matrix composite-response surface methodology approach. *Int J Adv Manuf Tech* 48: 613–624.
18. Gupta MK, Sood PK, Sharma VS (2016) Machining parameters optimization of titanium alloy using response surface methodology and particle swarm optimization under minimum-quantity lubrication environment. *Mater Manuf Process* 31: 1671–1682.
19. Kiaee N, Aghaie-Khafri M (2014) Optimization of gas tungsten arc welding process by response surface methodology. *Mater Design* 54: 25–31.
20. Vidyarthy RS, Dwivedi DK, Muthukumaran V (2018) Optimization of A-TIG process parameters using response surface methodology. *Mater Manuf Process* 33: 709–717.

21. Olivares EAG, D áz VMV (2018) Study of the hot-wire TIG process with AISI-316L filler material, analysing the effect of magnetic arc blow on the dilution of the weld bead. *Weld Int* 32: 139–148.
22. Bawazer LA, Ihli J, Comyn TP, et al. (2015) Genetic algorithm—Guided discovery of additive combinations that direct quantum dot assembly. *Adv Mater* 27: 223–227.
23. Nagaraju S, Vasantharaja P, Chandrasekhar N, et al. (2016) Optimization of welding process parameters for 9Cr-1Mo steel using RSM and GA. *Mater Manuf Process* 31: 319–327.
24. Radhika N, Raghu R (2018) Prediction of mechanical properties and modeling on sliding wear behavior of LM25/TiC composite using response surface methodology. *Particul Sci Technol* 36: 104–111.
25. Nageswaran G, Natarajan S, Ramkumar KR (2018) Synthesis, structural characterization, mechanical and wear behaviour of Cu-TiO_2-Gr hybrid composite through stir casting technique. *J Alloy Compd* 768: 733–741.
26. Ramkumar KR, Sivasankaran S, Alaboodi AS (2017) Effect of alumina content on microstructures, mechanical, wear and machining behavior of Cu-10Zn nanocomposite prepared by mechanical alloying and hot-pressing. *J Alloy Compd* 709: 129–141.
27. Thankachan T, Prakash KS, Loganathan M (2018) WEDM process parameter optimization of FSPed copper-BN composites. *Mater Manuf Process* 33: 350–358.
28. Jeyaprakash N, Duraiselvam M, Aditya SV (2018) Numerical modeling of WC-12% Co laser alloyed cast iron in high temperature sliding wear condition using response surface methodology. *Surf Rev Lett* 25: 1950009.

AIMS Press